Queensland University of Technology
Brisbane Australia

This may be the author's version of a work that was submitted/accepted for publication in the following source:

Hao, Guolin, Kou, Liangzhi, Lu, Donglin, Peng, Jie, Li, Jin, Tang, Chao, & Zhong, Jianxin
(2016)
Electrostatic properties of two-dimensional WSe2 nanostructures.
Journal of Applied Physics, *119*(3), Article number: 035301 1-6.

This file was downloaded from: https://eprints.qut.edu.au/221608/

© Consult author(s) regarding copyright matters

This work is covered by copyright. Unless the document is being made available under a Creative Commons Licence, you must assume that re-use is limited to personal use and that permission from the copyright owner must be obtained for all other uses. If the document is available under a Creative Commons License (or other specified license) then refer to the Licence for details of permitted re-use. It is a condition of access that users recognise and abide by the legal requirements associated with these rights. If you believe that this work infringes copyright please provide details by email to qut.copyright@qut.edu.au

Notice: *Please note that this document may not be the Version of Record (i.e. published version) of the work. Author manuscript versions (as Submitted for peer review or as Accepted for publication after peer review) can be identified by an absence of publisher branding and/or typeset appearance. If there is any doubt, please refer to the published source.*

https://doi.org/10.1063/1.4940160

Electrostatic properties of two-dimensional WSe_2 nanostructures

Guolin Hao, Liangzhi Kou, Donglin Lu, Jie Peng, Jin Li, Chao Tang, and Jianxin Zhong

Citation: Journal of Applied Physics **119**, 035301 (2016); doi: 10.1063/1.4940160
View online: https://doi.org/10.1063/1.4940160
View Table of Contents: http://aip.scitation.org/toc/jap/119/3
Published by the American Institute of Physics

Articles you may be interested in

Band offsets and heterostructures of two-dimensional semiconductors
Applied Physics Letters **102**, 012111 (2013); 10.1063/1.4774090

Materials properties of out-of-plane heterostructures of MoS_2-WSe_2 and WS_2-$MoSe_2$
Applied Physics Letters **108**, 063105 (2016); 10.1063/1.4941755

2D-2D tunneling field-effect transistors using WSe_2/$SnSe_2$ heterostructures
Applied Physics Letters **108**, 083111 (2016); 10.1063/1.4942647

Surface potential and interlayer screening effects of few-layer MoS_2 nanoflakes
Applied Physics Letters **102**, 143110 (2013); 10.1063/1.4801844

Strain engineering in monolayer WS_2, MoS_2, and the WS_2/MoS_2 heterostructure
Applied Physics Letters **109**, 173105 (2016); 10.1063/1.4966218

Band alignment of two-dimensional transition metal dichalcogenides: Application in tunnel field effect transistors
Applied Physics Letters **103**, 053513 (2013); 10.1063/1.4817409

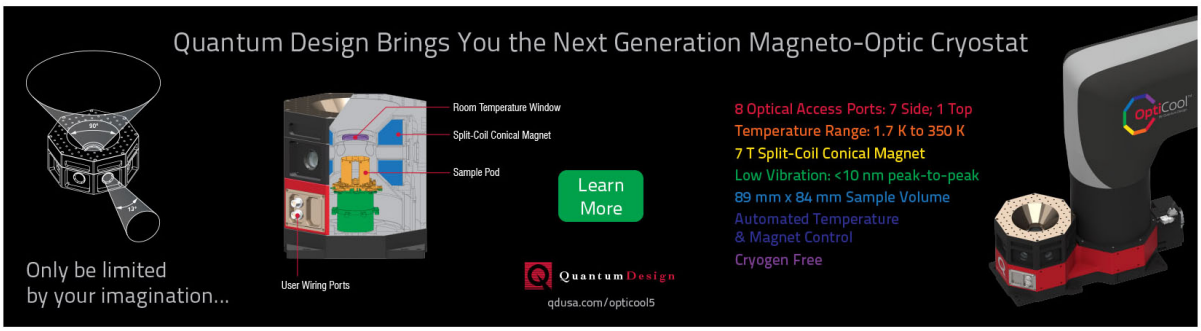

Electrostatic properties of two-dimensional WSe_2 nanostructures

Guolin Hao,[1,2,3,a)] Liangzhi Kou,[4] Donglin Lu,[1] Jie Peng,[1] Jin Li,[1] Chao Tang,[1,a)] and Jianxin Zhong[1,a)]
[1]*Hunan Key Laboratory for Micro-Nano Energy Materials and Devices, Xiangtan University, Hunan 411105, People's Republic of China*
[2]*State Key Laboratory of Silicon Materials, Zhejiang University, Hangzhou 310027, People's Republic of China*
[3]*Laboratory of Solid State Microstructures, Nanjing University, Nanjing 210093, People's Republic of China*
[4]*School of Chemistry, Physics and Mechanical Engineering Faculty, Queensland University of Technology, Garden Point Campus, QLD 4001 Brisbane, Australia*

(Received 4 October 2015; accepted 6 January 2016; published online 15 January 2016)

Recently, two-dimensional transition metal dichalcogenides have intrigued much attention due to their promising applications in optoelectronics. The electrostatic property investigation of WSe_2 nanostructures is essential for device application. Here, the interlayer screening effects of WSe_2 nanoplates with different thicknesses were investigated by measuring surface potential employing Kelvin probe force microscopy. Simultaneously, charges can be injected into WSe_2 nanoplate by means of conducting atomic force microscopy to tune the electrostatic properties of WSe_2 nanostructures. Our experimental results have some important implications for improving performance of WSe_2-based optoelectronic devices through interface or surface engineering. © *2016 AIP Publishing LLC*. [http://dx.doi.org/10.1063/1.4940160]

I. INTRODUCTION

Since the discovery of graphene in 2004,[1] two-dimensional (2D) materials have attracted tremendous attention due to their fascinating physics and promising applications in the next generation electronics and optoelectronics.[2–5] Although graphene is by far the most extensively studied two-dimensional material, its practical applications are greatly limited in semiconducting and photonic devices due to the lack of band gap.[6] Therefore, semiconductors with relatively large band gap are essential for fabricating field effect transistors with high current on/off ratio and low power consumption, which motivate researchers to explore more promising 2D atomic crystals with nonzero band gap.[7–10] 2D transition metal dichalcogenides (TMDs) are promising candidates, which have the form of MX_2 (M = Mo and W; X = S, Te, and Se) and intrinsic band gap.[4,11,12] MX_2 has an indirect band gap in the bulk form, but turns to be direct when reducing the thickness to monolayer due to quantum confinement effect.[4] Such unique electronic properties offer unprecedented opportunities and have wide applications in electronics, valleytronics, as well as optoelectronic fields.[4,13–16] As a typical example of MX_2, recent studies have demonstrated that monolayer WSe_2 nanostructure has a smaller band gap (~1.7 eV) and exhibits excellent mobility (~250 $cm^2\ V^{-1}\ s^{-1}$) and high current on/off ratio (~10^8) at room temperature, which make it of great interest for electronic and optoelectronic devices.[17–19]

Unlike single atomic layer graphene, each charge neutralized WSe_2 layer is formed by three covalently bonded atomic layers in the sequence of Se-W-Se with thickness of ~0.7 nm (Figure 1(a)). It is dominated by weak van der Waals interactions between the neighboring sandwich layers, which makes it easily be obtained through micro- mechanical cleavage and exfoliation methods as well as liquid phase intercalation.[20,21] Besides the mechanical method, the growth of high quality large area WSe_2 nanostructures is also important and essential towards its engineering and integration of large-scale device applications.[22,23] On the other hand, a deep investigation on the charge and surface potential distribution as well as the electric screening effect is essential for designing and engineering MX_2-based optoelectronic devices with improved performance.[24,25] However, detailed investigation of electrostatic properties for monolayer and few-layer WSe_2 nanostructures is still missing.

Here, we report the synthesis of monolayer and few-layer WSe_2 nanostructures by vapor phase deposition method. The charge distribution and electrostatic screening effect of WSe_2 nanostructure with different layers have been investigated by Kelvin probe force microscopy (KPFM). We find that the surface potential of WSe_2 nanostructure increases and approaches the bulk value above 7 layers. We simultaneously provide a useful way to engineer the electrostatic properties of WSe_2 nanostructure by injecting charge carriers into the WSe_2 nanostructures.

II. EXPERIMENTAL DETAILS

The experimental setup is schematically shown in Figure 1(b). The source materials of high purity WSe_2 powders (99.95%) were used as the precursors and located in a 12 in. horizontal tube furnace. The *c*-oriented sapphire substrates were placed in the downstream at the expected regions for the growth of WSe_2 nanostructures. The furnace was heated to 950 °C in 30 min and maintained for 30 min, followed by naturally cooling down to room temperature. During growth, the pressure of the furnace is maintained at 80 Pa and the Ar/H_2 gas (Ar, 95%) is flowing at 40 sccm.

[a)]Electronic addresses: guolinhao@xtu.edu.cn, tang_chao@xtu.edu.cn, and jxzhong@xtu.edu.cn

 © 2016 AIP Publishing LLC

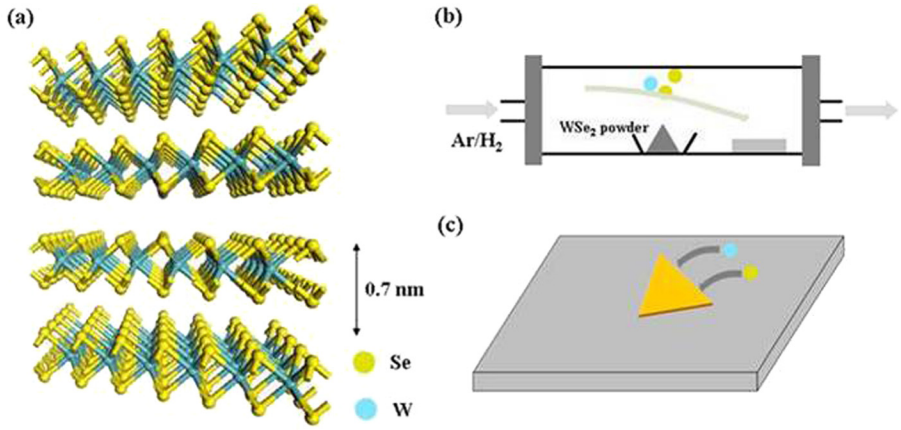

FIG. 1. (a) Crystal structure of WSe_2 with each layer formed by W and Se atomic sheets. (b) A schematic drawing of WSe_2 nanostructure growth in a horizontal tube furnace and the model of corresponding growth mechanism.

The morphologies and nanostructures of synthesized WSe_2 samples are systematically characterized by using optical microscopy and atomic force microscopy (AFM, SEIKO, SPI3800N + 300 HV). Raman spectra and photoluminescence (PL) properties of WSe_2 nanostructures were excited at room temperature by using Renishaw in Via micro-Raman spectrometer. The electrostatic properties of WSe_2 nanostructures and charge injection were investigated by KPFM and conducting AFM (SPM, SEIKO, SPI3800N + 300 HV).

III. RESULTS AND DISCUSSIONS

The morphologies of synthesized products grown on the *c*-oriented sapphire (Al_2O_3) substrates are systematically investigated, which are strongly dependent on growth conditions. Figure 2 shows an optical image of WSe_2 nanostructures grown 12 cm away from the hot center. It can be seen that high density of large area WSe_2 nanoplates (NPs) are merged together forming ultrathin continuous films with lateral dimensions up to centimeter scale, as depicted in Figure 2(a). The inset shows a photo image of sapphire substrates before and after the growth of WSe_2 nanostructures over centimeter length scale. In Figures 2(b)–2(d), we show the separate large-scale ultrathin WSe_2 NPs with uniform monolayer thickness, which were obtained at the distance 14 cm away from the hot center, they usually exhibit flower-like morphologies with lateral sizes from several tens of micrometers up to 50 μm. At the place of farther away from the center (~16 cm), the WSe_2 NPs with smaller lateral sizes can be obtained. The thickness and morphology of synthesized WSe_2 ultrathin NPs are measured by AFM. Figure 2(e) is a typical AFM image of flower-like monolayer WSe_2 NP with uniform surface, thickness of ~0.84 nm, which corresponds to the monolayer WSe_2 NP. AFM height topography measurements confirm that most of the WSe_2 NPs are single-layered. The WSe_2 layer with uniform thickness and minimal roughness is essential for obtaining high performance of WSe_2-based devices. Meanwhile, grain boundaries in monolayer WSe_2 nanostructures are also clearly observed (Figure 2(f)).

Raman spectroscopy is an effective method for the characterization of the crystal quality in two-dimensional materials.[19] Room temperature Raman spectroscopy of monolayer WSe_2 was obtained by using a 532 nm laser operated at a low power level (~0.01 mW). As shown in Figure 3(a), $E_{2g}{}^1$ and A_{1g} phonon modes of monolayer WSe_2 NP were observed at 253 cm^{-1} and 263 cm^{-1}, respectively, which are consistent with the previous report.[22] To investigate the PL properties, PL spectroscopy of different thicknesses of WSe_2 NPs is characterized with a 532 nm excitation wavelength. Monolayer WSe_2 NP exhibits a relatively sharp and strong intensity peak at ~741 nm (as shown in Figure 3(b)). Under the same measured conditions, tri-layer WSe_2 NPs shows a very weak PL signal at 775 nm. For multilayer WSe_2 samples, extremely weak PL signal can be hardly found. Corresponding optical image of WSe_2 NPs with different thicknesses is displayed in the inset of Figure 3(b). Our experiments demonstrate a direct band gap for monolayer WSe_2 NP.

Previous reports have demonstrated that the c-oriented sapphire is a good van der Waals epitaxy substrate for the growth of two-dimensional atomic crystals.[26] Although the lattice mismatch of WSe_2 and sapphire substrate is 44.9%, the in-plane lattice can be reduced to 8.7% with 4a (WSe_2) = 1.3128 nm and 3a (c-sapphire) = 1.4274 nm. The epitaxial growth of van der Waals materials can be obtained on a relatively large lattice mismatch compared with the other traditional epitaxy. Figure 4(a) shows the AFM image of sapphire substrate surface. During our experiment, we found that a large number of atomic steps with width of ~100 nm can be recognized on the (0001)-oriented sapphire substrate surface after annealing (Figure 4(b)). Nevertheless, few reports for the growth of two-dimensional materials have considered the atomic step sapphire substrate. We believe that the WSe_2 nanostructures are formed preferentially on the atomic step at the sapphire surface. As a result, the monolayer WSe_2 NP surface in Figures 4(c) and 4(d) exhibits terrace structures.

Due to the excellent electronic and optical properties of WSe_2 nanostructures, a variety of two-dimensional WSe_2-based devices, such as field effect transistors, photodetectors and sensors, have been demonstrated and fabricated, which make it of great interest for the practical applications.[4] However, these applications indicate that WSe_2 nanostructures are supported on substrates. A deep insight into the surface potential and charge distribution as well as electric field screening of WSe_2 NPs with different number of layers and quantitative understanding of charge transfer at the interface

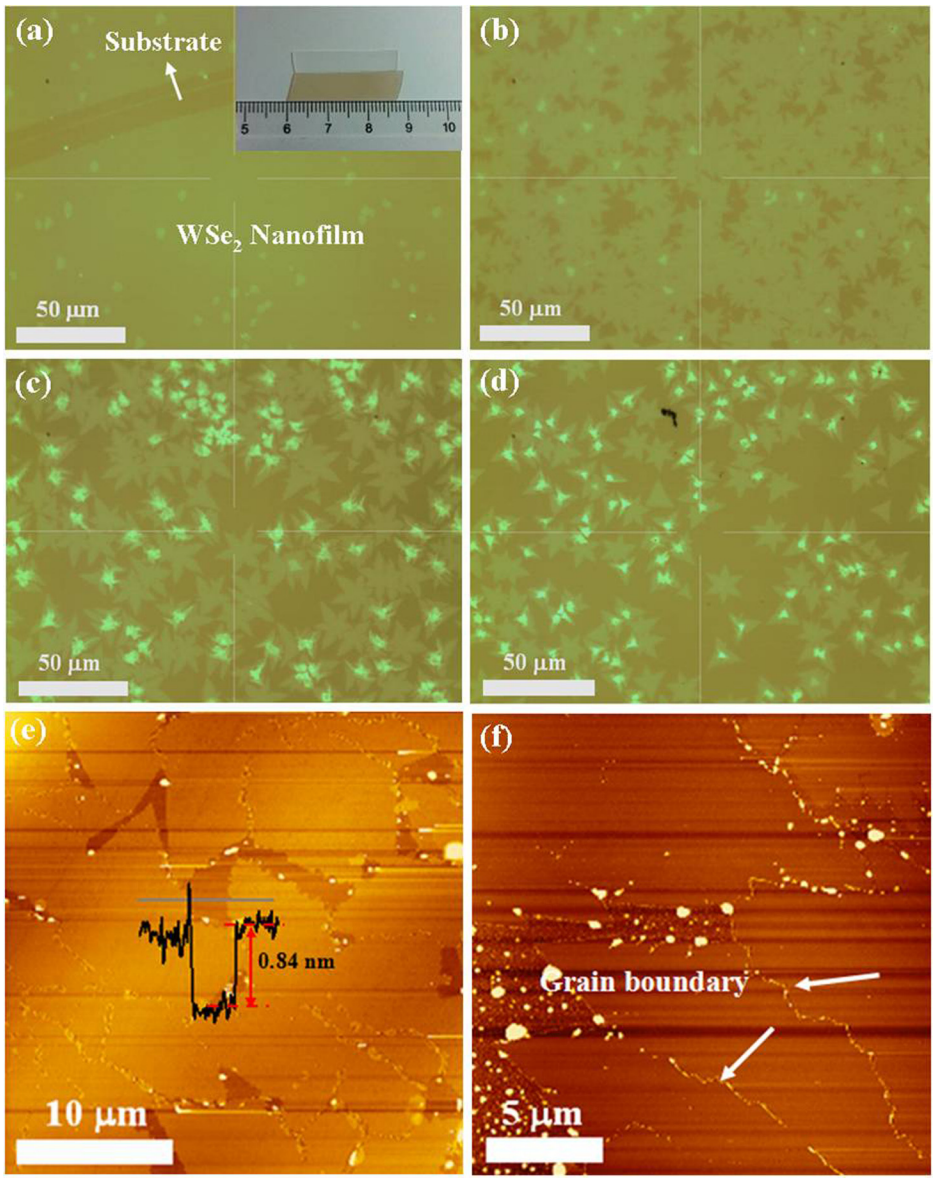

FIG. 2. (a) Optical image of as-prepared WSe_2 nanostructure. Inset: the optical image of sapphire substrate before and after the growth of WSe_2 nanostructures. (b)-(d) Optical images of WSe_2 NPs. (e) and (f) Corresponding AFM images of monolayer WSe_2 NPs.

are crucial for device design and the improving performance of WSe_2-based devices. Nevertheless, little attention has been focused on the electrostatic screening properties of WSe_2 nanostructures. KPFM is a versatile and spatially precise method for detecting surface potential and charge distribution, molecular doping, and charge transfer at the interface of low dimensional materials.[26–29] Here, the surface potential and charge distributions have been systematically characterized by measuring contact potential difference (CPD) between AFM tips and WSe_2 samples using KPFM technique. CPD is defined as

$$CPD = \frac{\Phi_{tip} - \Phi_{sample}}{e},$$

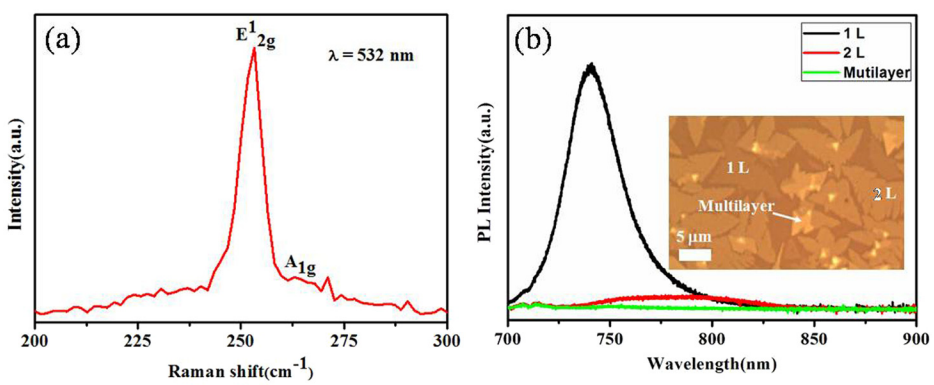

FIG. 3. (a) Raman spectroscopy of monolayer WSe_2 NP growing on sapphire substrate. (b) PL spectra of WSe_2 NPs with different thicknesses.

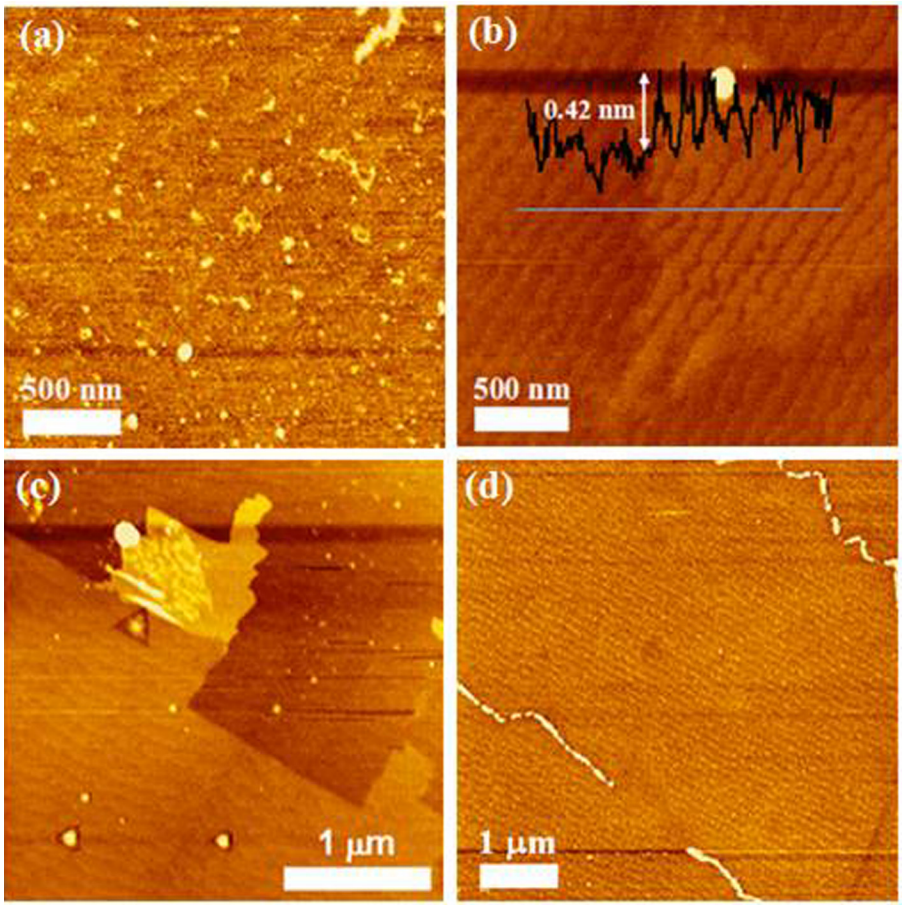

FIG. 4. (a) AFM image of sapphire substrate before annealing. (b) Corresponding AFM image of sapphire substrate after annealing exhibiting atomic steps. (c) and (d) Typical AFM images of synthesized WSe_2 nanostructures.

where Φ_{tip} and Φ_{sample} are the work function of the tip and the sample, respectively. KPFM experiments are conducted in ambient conditions by using MikroMasch CSC-17/Cr-Au tips with a force constant of 0.15 N/m. In our experiment, we employ single-pass mode to acquire both the topography and surface potential information simultaneously without losing measurement sensitivity. For the measurement of electrostatic properties, an AC voltage (~8 V) and frequency (11.8 kHz) were applied to the KPFM tip.

Figures 5(a) and 5(b) are the topography of WSe_2 nanostructures with different thicknesses, and the corresponding surface potential image is shown in Figure 5(c). It can be clearly seen that surface potential on the same layer of a WSe_2 NP are relatively uniform (less than 10 mV), indicating the high quality of WSe_2 samples without obvious defect or charge impurities in the WSe_2 surface. The surface potential for the monolayer WSe_2 NP was approximately −35 mV. However, the surface potential exhibits remarkable contrast between different number of layers. As shown in Figure 5(d), the value of trilayer WSe_2 surface potential is 40 mV higher than the monolayer WSe_2. By measuring a number of WSe_2 samples, the surface potential behavior of different layers relative to bulk WSe_2 is obtained. As shown in Figure 5(d), the screening effect of WSe_2 NPs is obvious. The surface potential increased monotonically with the thickness and approached a bulk value for 7 or more WSe_2 layers. We propose that the observed potential variation of WSe_2 between different layers is originated from the charge transfer at the WSe_2/sapphire interface, which is not completely screened by the atomically thin WSe_2 samples. The lower surface potential of monolayer WSe_2 with respect to bulk WSe_2 is the result of electron depletion in WSe_2, which indicates p-doping from sapphire substrates to monolayer or few-layer WSe_2 NPs. However, the eventual performance of WSe_2-based devices also depends on its initial carrier concentration. Our experimental results provide an important indication to modify the electronic and optical properties of WSe_2-based devices by choosing suitable substrates.

In order to investigate the electrostatic property engineering of WSe_2 nanostructures, charge injection experiment was achieved by using conductive AFM with a gold-coated Si probe (CSC-17/Cr-Au) of force constant of 0.15 N/m. The conductive tip is biased at V_{inj} with respect to substrate and the injection time is maintained for 2 min. During charge injection on a given WSe_2 nanoplate, the contact force is maintained as ~2 nN. Once the charge injection is finished, corresponding surface potential measurements are characterized by using KPFM. Figures 6(a) and 6(b) are the surface potential images of one typical monolayer WSe_2 NP before and after electron injection under the bias of 6 V, which both exhibit uniform surface potential distribution. The surface potential dependence on the charge injection bias voltage (V_{inj}) was also investigated. Figure 4(c) shows the surface potential measurements as a function of V_{inj}. It is interesting to note that surface potential values can be tuned by applying different negative charge biases. Our experimental results indicate that the electrons can be successfully injected into the WSe_2 NP. However, we found that the positive charges are very difficult to be injected into the WSe_2 NP, which

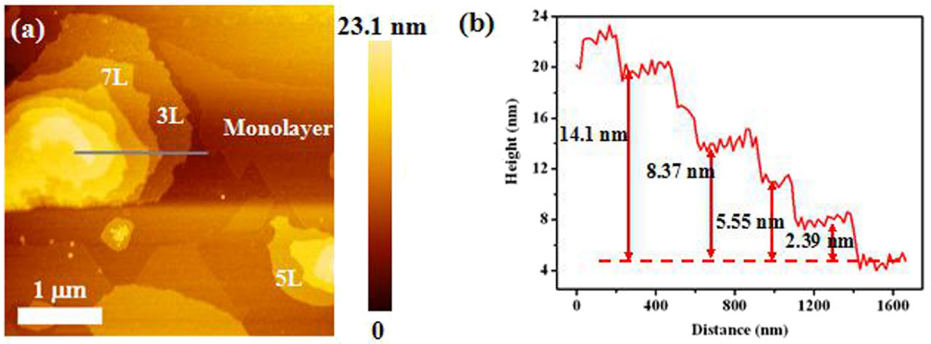

FIG. 5. (a) Typical AFM images of WSe_2 nanostructures with different thicknesses. (b) Height profile corresponding to the line in Fig. 6(a). (c) Corresponding surface potential image exhibiting homogeneous distribution on each same layer. (d) The surface potential value of WSe_2 nanostructures with different thicknesses. The error bars are calculated from average values of 5 samples.

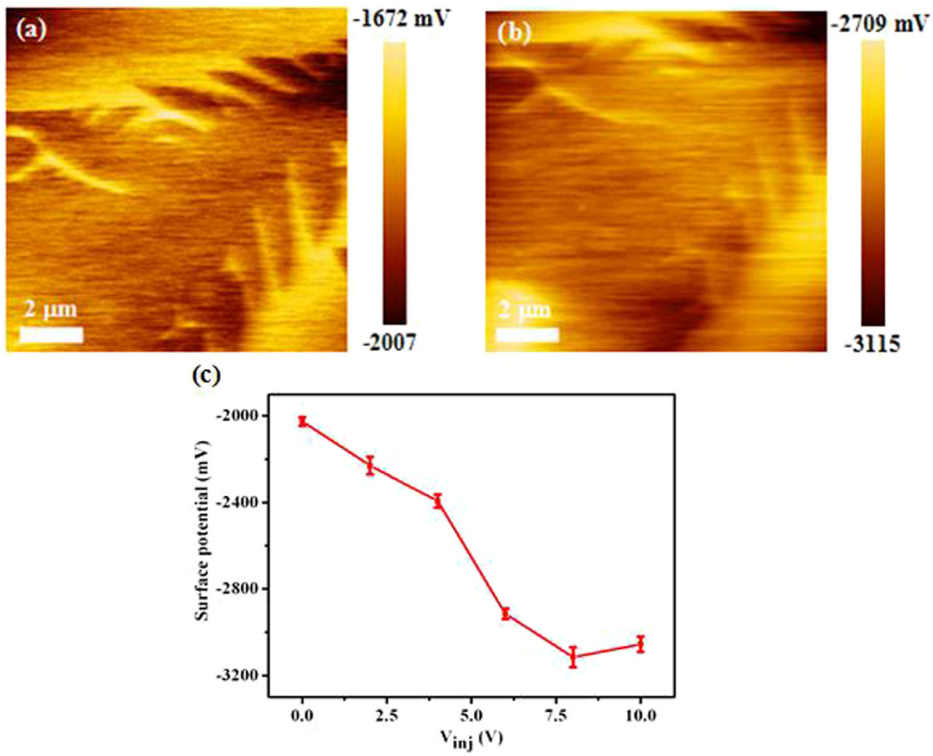

FIG. 6. (a) Surface potential of Wse_2 nanoplate before charge injection. (b) Corresponding surface potential under charge injection under the charge injection bias of 6 V. (c) Surface potential as a function of V_{inj} after electron injection. The error bars correspond to standard deviations from the average values of 3 samples.

may be due to the p-type doping nature of WSe_2 nanostructures fabricated during the growth process by vapor phase deposition method.

IV. CONCLUSION

In summary, the electrostatic properties of WSe_2 nanostructures are systematically investigated. Screening effect of WSe_2 nanostructures by measuring surface potential and charge distribution was investigated. Surface potential of WSe_2 nanostructures is found to increase with the number of WSe_2 layers suggesting screening effect due to the charge exchange at the interface between WSe_2 and substrates. The electrons can be easily injected into the WSe_2 NP by controlling the charge injection bias, which is a useful way to engineer the electrostatic properties of WSe_2 nanostructures.

ACKNOWLEDGMENTS

This work was supported by Grants from National Natural Science Foundation of China (Nos. 11404274, 11474244, 11404275, 51172191, and 11204260), the General Project of

the Education Department of Hunan Province (No. 14C1096), Natural Science Foundation of Hunan Province (No. 2015JJ3118), the Program for Changjiang Scholars and Innovative Research Team in University (No. IRT13093), and National Basic Research Program of China (No. 2012CB921303).

[1]K. S. Novoselov, A. K. Geim, S. V. Morozov, D. Jiang, Y. Zhang, S. V. Dubonos, I. V. Grigorieva, and A. A. Firsov, Science **306**(5696), 666–669 (2004).
[2]M. Xu, T. Liang, M. Shi, and H. Chen, Chem. Rev. **113**(5), 3766–3798 (2013).
[3]K. S. Novoselov, D. Jiang, F. Schedin, T. J. Booth, V. V. Khotkevich, S. V. Morozov, and A. K. Geim, Proc. Natl. Acad. Sci. U.S.A. **102**(30), 10451–10453 (2005).
[4]Q. H. Wang, K. Kalantar-Zadeh, A. Kis, J. N. Coleman, and M. S. Strano, Nat. Nanotechnol. **7**(11), 699–712 (2012).
[5]S. Z. Butler, S. M. Hollen, L. Cao, Y. Cui, J. A. Gupta, H. R. Gutiérrez, T. F. Heinz, S. S. Hong, J. Huang, A. F. Ismach, E. Johnston-Halperin, M. Kuno, V. V. Plashnitsa, R. D. Robinson, R. S. Ruoff, S. Salahuddin, J. Shan, L. Shi, M. G. Spencer, M. Terrones, W. Windl, and J. E. Goldberger, ACS Nano **7**(4), 2898–2926 (2013).
[6]R. Balog, B. Jorgensen, L. Nilsson, M. Andersen, E. Rienks, M. Bianchi, M. Fanetti, E. Laegsgaard, A. Baraldi, S. Lizzit, Z. Sljivancanin, F. Besenbacher, B. Hammer, T. G. Pedersen, P. Hofmann, and L. Hornekaer, Nat. Mater. **9**(4), 315–319 (2010).
[7]S. Das, H.-Y. Chen, A. V. Penumatcha, and J. Appenzeller, Nano Lett. **13**(1), 100–105 (2013).
[8]S. Kim, A. Konar, W.-S. Hwang, J. H. Lee, J. Lee, J. Yang, C. Jung, H. Kim, J.-B. Yoo, J.-Y. Choi, Y. W. Jin, S. Y. Lee, D. Jena, W. Choi, and K. Kim, Nat. Commun. **3**, 1011 (2012).
[9]H. B. Zeng, C. Y. Zhi, Z. H. Zhang, X. L. Wei, X. B. Wang, W. L. Guo, Y. Bando, and D. Golberg, Nano Lett. **10**(12), 5049–5055 (2010).
[10]S. L. Zhang, Z. Yan, Y. F. Li, Z. F. Chen, and H. B. Zeng, Angew. Chem. Int. Ed. **127**(10), 3155–3158 (2015).
[11]M. Chhowalla, H. S. Shin, G. Eda, L.-J. Li, K. P. Loh, and H. Zhang, Nat. Chem. **5**(4), 263–275 (2013).
[12]D. Jariwala, V. K. Sangwan, L. J. Lauhon, T. J. Marks, and M. C. Hersam, ACS Nano **8**(2), 1102–1120 (2014).
[13]W. Bao, X. Cai, D. Kim, K. Sridhara, and M. S. Fuhrer, Appl. Phys. Lett. **102**(4), 042104 (2013).
[14]D. Xiao, G.-B. Liu, W. Feng, X. Xu, and W. Yao, Phys. Rev. Lett. **108**(19), 196802 (2012).
[15]X. Xu, W. Yao, D. Xiao, and T. F. Heinz, Nat. Phys. **10**(5), 343–350 (2014).
[16]B. Radisavljevic, A. Radenovic, J. Brivio, V. Giacometti, and A. Kis, Nat. Nanotechnol. **6**(3), 147–150 (2011).
[17]W. Liu, J. Kang, D. Sarkar, Y. Khatami, D. Jena, and K. Banerjee, Nano Lett. **13**(5), 1983–1990 (2013).
[18]H. Zhou, C. Wang, J. C. Shaw, R. Cheng, Y. Chen, X. Huang, Y. Liu, N. O. Weiss, Z. Lin, Y. Huang, and X. Duan, Nano Lett. **15**(1), 709–713 (2015).
[19]P. Tonndorf, R. Schmidt, P. Böttger, X. Zhang, J. Börner, A. Liebig, M. Albrecht, C. Kloc, O. Gordan, D. R. T. Zahn, S. Michaelis de Vasconcellos, and R. Bratschitsch, Opt. Express **21**(4), 4908–4916 (2013).
[20]H. Li, G. Lu, Y. Wang, Z. Yin, C. Cong, Q. He, L. Wang, F. Ding, T. Yu, and H. Zhang, Small **9**(11), 1974–1981 (2013).
[21]J. N. Coleman, M. Lotya, A. O'Neill, S. D. Bergin, P. J. King, U. Khan, K. Young, A. Gaucher, S. De, R. J. Smith, I. V. Shvets, S. K. Arora, G. Stanton, H.-Y. Kim, K. Lee, G. T. Kim, G. S. Duesberg, T. Hallam, J. J. Boland, J. J. Wang, J. F. Donegan, J. C. Grunlan, G. Moriarty, A. Shmeliov, R. J. Nicholls, J. M. Perkins, E. M. Grieveson, K. Theuwissen, D. W. McComb, P. D. Nellist, and V. Nicolosi, Science **331**(6017), 568–571 (2011).
[22]J.-K. Huang, J. Pu, C.-L. Hsu, M.-H. Chiu, Z.-Y. Juang, Y.-H. Chang, W.-H. Chang, Y. Iwasa, T. Takenobu, and L.-J. Li, ACS Nano **8**(1), 923–930 (2014).
[23]K. Xu, Z. Wang, X. Du, M. Safdar, C. Jiang, and J. He, Nanotechnology **24**(46), 465705 (2013).
[24]Y. Li, C.-Y. Xu, and L. Zhen, Appl. Phys. Lett. **102**(14), 143110 (2013).
[25]S. W. Luo, G. L. Hao, Y. P. Fan, L. Z. Kou, C. Y. He, X. Qi, C. Tang, J. Li, K. Huang, and J. X. Zhong, Nanotechnology **26**(10), 105705 (2015).
[26]A. E. Curtin, M. S. Fuhrer, J. L. Tedesco, R. L. Myers-Ward, C. R. Eddy, and D. K. Gaskill, Appl. Phys. Lett. **98**(24), 243111 (2011).
[27]G. L. Hao, X. Qi, Y. P. Fan, L. Xue, X. Y. Peng, X. L. Wei, and J. X. Zhong, Appl. Phys. Lett. **102**(1), 013104–013105 (2013).
[28]A. Castellanos-Gomez, E. Cappelluti, R. Roldán, N. Agraït, F. Guinea, and G. Rubio-Bollinger, Adv. Mater. **25**(6), 899–903 (2013).
[29]M. Yamamoto, S. Dutta, S. Aikawa, S. Nakaharai, K. Wakabayashi, M. S. Fuhrer, K. Ueno, and K. Tsukagoshi, Nano Lett. **15**(3), 2067–2073 (2015).